

Accuracy Progressive Calculation of Lagrangian Trajectories from a Gridded Velocity Field

PETER C. CHU AND CHENWU FAN

Naval Ocean Analysis and Prediction Laboratory, Department of Oceanography, Naval Postgraduate School, Monterey, California

(Manuscript received 29 September 2013, in final form 21 January 2014)

ABSTRACT

Reduction of computational error is a key issue in computing Lagrangian trajectories using gridded velocities. Computational accuracy enhances from using the first term (constant velocity scheme), the first two terms (linear uncoupled scheme), the first three terms (linear coupled scheme), to using all four terms (nonlinear coupled scheme) of the two-dimensional interpolation. A unified “analytical form” is presented in this study for different truncations. Ordinary differential equations for predicting Lagrangian trajectory are linear using the constant velocity/linear uncoupled schemes (both commonly used in atmospheric and ocean modeling), the linear coupled scheme, and the nonlinear using the nonlinear coupled scheme (both proposed in this paper). The location of the Lagrangian drifter inside the grid cell is determined by two algebraic equations that are solved explicitly with the constant velocity/linear uncoupled schemes, and implicitly using the Newton–Raphson iteration method with the linear/nonlinear coupled schemes. The analytical Stommel ocean model on the f plane is used to illustrate great accuracy improvement from keeping the first term to keeping all the terms of the two-dimensional interpolation.

1. Introduction

Oceanic and atmospheric motion can be represented by Eulerian and Lagrangian viewpoints. The former gives time-dependent three-dimensional (Eulerian) fields of velocity, temperature, salinity, and other variables, which are commonly represented in satellite observations, modeling, simulation, and prediction at numerical grid points. The latter provides continually changing characteristics (temperature, salinity, velocity, etc.) along the fluid particles’ trajectories (i.e., Lagrangian trajectories), which are commonly represented in situ oceanographic measurements by Argo floats, drifters, and gliders. Employing the Lagrangian trajectories, water masses can also be distinguished in terms of origin and/or destination and can be traced (Vries and Doos 2001). The two types of velocity are convertible. Routine ocean data assimilation systems (Galanis et al. 2006; Lozano et al. 1996; Song and Colberg 2011; Sun 1999) and data analysis methods, such as optimal

interpolation (OI) (Gandin 1965) and optimal spectral decomposition (OSD) (Chu et al. 2003a,b), can be used for converting Lagrangian drifter data into gridded Eulerian-type data, and for evaluating ocean models (e.g., Chu et al. 2001, 2004). Several new phenomena were discovered after the conversion. For example, with the OSD method new signals have been identified, such as fall–winter recurrence of current reversal from westward to eastward on the Texas–Louisiana continental shelf from near-surface drifting buoy and current meter (Chu et al. 2005), and propagation of long baroclinic Rossby waves at middepth (around 1000 m deep) in the tropical North Atlantic from the Argo floats (Chu et al. 2007).

Consider water particles flowing with ocean currents in three-dimensional space (x, y, z) and time t , discretized into grid cells with the spacing of $(\Delta x, \Delta y, \Delta z)$ and time step of Δt , with the discrete Eulerian velocity field represented by

$$\hat{\mathbf{v}}(x_i, y_j, z_k, t_l) = [\hat{u}(x_i, y_j, z_k, t_l), \hat{v}(x_i, y_j, z_k, t_l), \hat{w}(x_i, y_j, z_k, t_l)]. \quad (1a)$$

Here, the subscripts (i, j, k, l) represent the spatial and temporal discretization. The superscript caret ($\hat{\cdot}$) means the Eulerian gridded fields. Common interpolation

Corresponding author address: Peter C. Chu, Naval Ocean Analysis and Prediction Laboratory, Department of Oceanography, Naval Postgraduate School, 833 Dyer Road, Monterey, CA 93943. E-mail: pcchu@nps.edu

methods can be used to get four-dimensional continuous velocity field from the gridded field (1a),

$$\mathbf{v}(x, y, z, t) = [u(x, y, z, t), v(x, y, z, t), w(x, y, z, t)]. \quad (1b)$$

The position of each fluid particle, $\mathbf{R}(t) = [x(t), y(t), z(t)]$, is specified in the Lagrangian system. The connection between the Eulerian and Lagrangian approaches leads to the ordinary differential equations,

$$\begin{aligned} \frac{dx(t)}{dt} &= u(x, y, z, t), & \frac{dy(t)}{dt} &= v(x, y, z, t), \\ \frac{dz(t)}{dt} &= w(x, y, z, t), \end{aligned} \quad (2a)$$

which determine the trajectory of the particle if the position is specified at some initial instant in its path history. Such calculation has also been used as the semi-Lagrangian scheme in ocean numerical modeling (e.g., Chu and Fan 2010). Thus, the interpolation (1b) is the key in calculating Lagrangian trajectories from gridded velocity fields. For steady gridded velocity fields, the analytical solution exists for the Lagrangian trajectory (2a) inside one grid cell with (1b) a highly truncated linear interpolation in space (see section 2 for explanation) (Doos 1995; Blanke and Raynaud 1997). Follow-up research has been extended from steady to unsteady velocity fields with the Lagrangian trajectories being calculated from time-varying gridded velocity fields (Vries and Doos 2001).

Two sources of uncertainty exist in determining the Lagrangian trajectories from the Eulerian flow field: (i) the knowledge of the smoothness and (ii) the error in the integration of the ordinary differential equations [(2a)]. There is a need to estimate uncertainties due to the limited knowledge of the Eulerian velocity (see section 2). To illustrate this point, consider the case that we only have access to the average of the velocity in a cell. In this case the trajectories within the cell are straight lines, called the constant velocity (CV) scheme. With more knowledge about the Eulerian velocity, for example, Vries and Doos (2001) used low-order truncation in spatial interpolation [see (5a) and (5b) in section 2] to simplify $[u(x, y, z, t), v(x, y, z, t)]$ in (2a) by

$$\begin{aligned} \frac{dx(t)}{dt} &= L_1(x, t) = \alpha_0 + \alpha_2 t + (\alpha_1 + \alpha_3 t)x, \\ \frac{dy(t)}{dt} &= L_2(y, t) = \beta_0 + \beta_2 t + (\beta_1 + \beta_3 t)y, \end{aligned} \quad (2b)$$

where u depends on (x, t) only and v depends on (y, t) only. Such a treatment leads to the existence of analytical solutions. The following coefficients in (2b) vanish

$$\alpha_2 = \alpha_3 = \beta_2 = \beta_3 = 0$$

when the Eulerian flow field is steady. The two functions in (2b) are represented by

$$\begin{aligned} L_1(x, t) &= \bar{L}_1(x) = \alpha_0 + \alpha_1 x, \\ L_2(y, t) &= \bar{L}_2(y) = \beta_0 + \beta_1 y. \end{aligned} \quad (2c)$$

In reality, for a 2D Eulerian flow field, the velocity components $u(x, y, t)$, and $v(x, y, t)$ in (2a) are not necessarily taken as the functions (L_1, L_2) given by (2b). Questions arise: What is the Lagrangian trajectory if the Eulerian velocity components (u, v) depend on (x, y) [more realistic]? Is there any improvement with such a change? In other words, what is the improvement for a steady Eulerian flow field if $\bar{L}_1(x)$ is changed into $u(x, y)$ and $\bar{L}_2(y)$ is changed into $v(x, y)$? What is the improvement for an unsteady Eulerian flow field if $L_1(x, t)$ is changed into $u(x, y, t)$ and $L_2(y, t)$ is changed into $v(x, y, t)$ for an unsteady Eulerian flow field? To show the accuracy progressive in the calculation of Lagrangian trajectories, a systematical analysis is presented in this study for a steady Eulerian flow field and will be presented in another paper in the near future for an unsteady Eulerian flow field. Division of steady and unsteady Eulerian flow fields is due to the mathematical complexity.

The rest of the paper is outlined as follows. Section 2 describes the establishment of continuous velocity inside a grid cell. Section 3 depicts the calculation of Lagrangian trajectory from side to side of a grid cell. Section 4 shows the identification of a starting grid cell. Section 5 describes the Lagrangian trajectory across the grid cell. Section 6 introduces the Stommel ocean model for the evaluation. Section 7 shows the accuracy progressive from high to no truncation of the two-dimensional interpolation. Section 8 presents the conclusions.

2. Establishment of continuous velocity inside a gridded cell

For simplicity without loss of generality, a steady-state two-dimensional gridded data cell is considered. Let the water particle be located at (called a starting point, not necessary at the grid point) $\mathbf{R}_0 = (x_0, y_0)$ inside the grid cell $[x_i \leq x_0 \leq x_{i+1}, y_j \leq y_0 \leq y_{j+1}]$ and let it move using the gridded data. Because of spatial variability of the gridded velocity data, the Lagrangian velocity changes with time although the Eulerian flow is steady. Let the velocity be given at the four corner points of the grid cell, $F_{i,j}, F_{i+1,j}, F_{i,j+1}, F_{i+1,j+1}$. Here, F represents (u, v) . For a two-dimensional interpolation, the velocities inside the ij grid cell can be given by the corner points,

$$F(x, y) = a_0 + a_1(x - x_{i-1}) + a_2(y - y_{j-1}) + a_3(x - x_{i-1})(y - y_{j-1}). \tag{3}$$

$$u(x, y) - u(x_0, y_0) = \frac{u(x_1, y_1) - u(x_0, y_0)}{x_1 - x_0}(x - x_0), \tag{4a}$$

Let the Lagrangian drifter travel from (x_0, y_0) to (x_1, y_1) with the travel time of τ (Fig. 1), and let the Lagrangian velocity components $u(x, y)$ and $v(x, y)$ be represented by

$$v(x, y) - v(x_0, y_0) = \frac{v(x_1, y_1) - v(x_0, y_0)}{y_1 - y_0}(y - y_0). \tag{4b}$$

Substitution of (3) into (4a) and (4b) leads to

$$\begin{aligned} u(x, y) - u(x_0, y_0) &= \frac{1}{x_1 - x_0} \left[u(x_0, y_0) \left(1 - \frac{x_1 - x_0}{\delta x}\right) \left(1 - \frac{y_1 - y_0}{\delta y}\right) + u(x_{i+1}, y_0) \frac{x_1 - x_0}{\delta x} \left(1 - \frac{y_1 - y_0}{\delta y}\right) \right. \\ &\quad \left. + u(x_0, y_{j+1}) \left(1 - \frac{x_1 - x_0}{\delta x}\right) \frac{y_1 - y_0}{\delta y} + u(x_{i+1}, y_{j+1}) \frac{x_1 - x_0}{\delta x} \frac{y_1 - y_0}{\delta y} - u(x_0, y_0) \right] (x - x_0) \\ &= \left\{ \frac{u(x_{i+1}, y_0) - u(x_0, y_0)}{\delta x} + \frac{u(x_0, y_{j+1}) - u(x_0, y_0)}{\delta y} \frac{y_1 - y_0}{x_1 - x_0} + \frac{y_1 - y_0}{\delta x \delta y} [u(x_0, y_0) - u(x_{i+1}, y_0) \right. \\ &\quad \left. - u(x_0, y_{j+1}) + u(x_{i+1}, y_{j+1})] \right\} (x - x_0) = \left[\left(\frac{\Delta u}{\Delta x}\right)_0 + \left(\frac{\Delta u}{\Delta y}\right)_0 \frac{y_1 - y_0}{x_1 - x_0} + \frac{y_1 - y_0}{\delta x \delta y} \left(u_{ij} \frac{\delta x}{\Delta x} \frac{\delta y}{\Delta y} \right. \right. \\ &\quad \left. \left. - u_{i+1j} \frac{\delta x}{\Delta x} \frac{\delta y}{\Delta y} - u_{ij+1} \frac{\delta x}{\Delta x} \frac{\delta y}{\Delta y} + u_{i+1j+1} \frac{\delta x}{\Delta x} \frac{\delta y}{\Delta y} \right) \right] (x - x_0) \end{aligned}$$

$$= \left[\left(\frac{\Delta u}{\Delta x}\right)_0 + \left(\frac{\Delta u}{\Delta y}\right)_0 \frac{y_1 - y_0}{x_1 - x_0} + \left(\frac{\Delta^2 u}{\Delta x \Delta y}\right)_0 (y_1 - y_0) \right] (x - x_0), \tag{5a}$$

solution although it may be important in the case of strongly curved streamlines.

Equations (5a) and (5b) can be rewritten into a more general form,

$$\begin{aligned} v(x, y) - v(x_0, y_0) &= \left[\left(\frac{\Delta v}{\Delta y}\right)_0 + \left(\frac{\Delta v}{\Delta x}\right)_0 \frac{x_1 - x_0}{y_1 - y_0} + \left(\frac{\Delta^2 v}{\Delta x \Delta y}\right)_0 (x_1 - x_0) \right] (y - y_0), \end{aligned}$$

$$\begin{aligned} u(x, y) &= u(x_o, y_0) + A_x(x - x_0), \\ v(x, y) &= v(x_o, y_0) + A_y(y - y_0), \end{aligned} \tag{6}$$

where

$$\begin{aligned} A_x &= \left(\frac{\Delta u}{\Delta x}\right)_0 + \left(\frac{\Delta u}{\Delta y}\right)_0 \frac{y_1 - y_0}{x_1 - x_0} + \left(\frac{\Delta^2 u}{\Delta x \Delta y}\right)_0 (y_1 - y_0), \\ A_y &= \left(\frac{\Delta v}{\Delta y}\right)_0 + \left(\frac{\Delta v}{\Delta x}\right)_0 \frac{x_1 - x_0}{y_1 - y_0} + \left(\frac{\Delta^2 v}{\Delta x \Delta y}\right)_0 (x_1 - x_0). \end{aligned} \tag{7}$$

where

$$\begin{aligned} \left(\frac{\Delta F}{\Delta x}\right)_0 &= \frac{F(x_{i+1}, y_0) - F(x_0, y_0)}{\delta x}, \\ \left(\frac{\Delta F}{\Delta y}\right)_0 &= \frac{F(x_0, y_{j+1}) - F(x_0, y_0)}{\delta y}, \\ \left(\frac{\Delta^2 F}{\Delta x \Delta y}\right)_0 &= \frac{F_{ij} - F_{i+1j} - F_{ij+1} + F_{i+1j+1}}{\Delta x \Delta y}, \\ \delta x &= x_{i+1} - x_0, \quad \delta y = y_{j+1} - y_0 \end{aligned}$$

are given from the gridded velocities as well as the starting velocity $[u(x_0, y_0), v(x_0, y_0)]$ with the starting position (x_0, y_0) . Vries and Doos (2001) only keep the first term in the bracket of the right-hand side of each equation in (5a) and (5b), and argued that inclusion of last two terms was impossible to give a general analytical

Substitution of (6) into (2a) leads to

$$\frac{dx(t)}{dt} = u(x, y) = u(x_o, y_0) + A_x(x - x_0), \tag{8a}$$

$$\frac{dy(t)}{dt} = v(x, y) = v(x_o, y_0) + A_y(y - y_0), \tag{8b}$$

which have the following solutions:

$$\begin{aligned} x(t) &= x_0 + u(x_0, y_0)t, \\ y(t) &= y_0 + v(x_0, y_0)t, \quad \text{if } A_x = A_y = 0, \end{aligned} \tag{9}$$

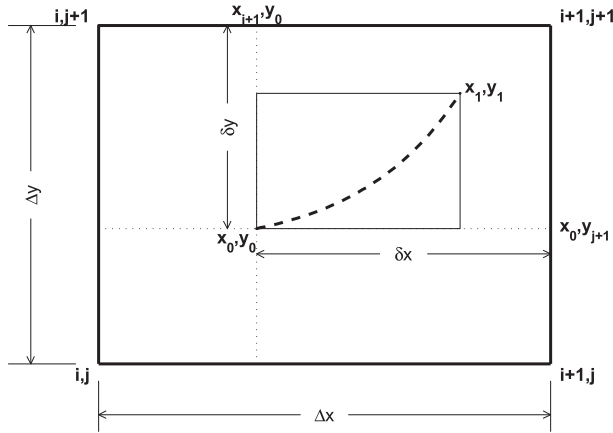


FIG. 1. Illustration of a Lagrangian trajectory $[x(t), y(t)]$ (dashed curve) from (x_0, y_0) to (x_1, y_1) inside the ij grid cell.

$$x(t) = x_0 + \frac{u(x_0, y_0)}{(\Delta u / \Delta x)_0} (e^{A_x t} - 1), \quad \text{if } A_x \neq 0, \quad (10a)$$

$$y(t) = y_0 + \frac{v(x_0, y_0)}{(\Delta v / \Delta y)_0} (e^{A_y t} - 1), \quad \text{if } A_y \neq 0. \quad (10b)$$

The solutions (9), (10a), and (10b) imply that the Lagrangian drifter never moves if the starting velocity equals zero, that is, $u_0 = u(x_0, y_0) = 0$ and $v_0 = v(x_0, y_0) = 0$.

For a sufficiently short travel time τ with the Lagrangian drifter still being inside the ij grid cell, the location (x_1, y_1) can be easily obtained if $A_x = 0, A_y = 0$, or (A_x, A_y) are given [i.e., keeping the first term in the right-hand side of (7)],

$$\begin{aligned} x_1 &= x_0 + u(x_0, y_0)\tau, \\ y_1 &= y_0 + v(x_0, y_0)\tau, \quad \text{if } A_x = 0, A_y = 0, \end{aligned} \quad (11a)$$

$$\begin{aligned} x_1 &= x_0 + \frac{u(x_0, y_0)}{(\Delta u / \Delta x)_0} (e^{A_x \tau} - 1), \\ y_1 &= y_0 + \frac{v(x_0, y_0)}{(\Delta v / \Delta y)_0} (e^{A_y \tau} - 1), \quad \text{if } A_x = \left(\frac{\Delta u}{\Delta x}\right)_0, \\ A_y &= \left(\frac{\Delta v}{\Delta y}\right)_0. \end{aligned} \quad (11b)$$

For more general cases [keeping the first two or all terms in the right-hand side of (7)], the location (x_1, y_1) satisfies the following two nonlinear algebraic equations:

$$x_1 = x_0 + \frac{u(x_0, y_0)}{(\Delta u / \Delta x)_0} \{\exp[A_x(x_1, y_1)]\tau - 1\}, \quad (12a)$$

$$y_1 = y_0 + \frac{v(x_0, y_0)}{(\Delta v / \Delta y)_0} \{\exp[A_y(x_1, y_1)]\tau - 1\}, \quad (12b)$$

which are solved by the Newton–Raphson iteration method.

3. Lagrangian trajectory from side to side of a grid cell

Various truncation of (3) leads to an accuracy increase in calculating the Lagrangian trajectory (inside the ij grid cell) from the gridded velocities at the four corners of the ij grid cell. If only the first term in the right-hand side of (3) is used—that is, $A_x = 0, A_y = 0$ —then the two ordinary differential equations [(8a) and (8b)] become

$$\frac{dx(t)}{dt} = u(x_0, y_0), \quad \frac{dy(t)}{dt} = v(x_0, y_0), \quad (13)$$

whose solutions are

$$x(t) = x_0 + u(x_0, y_0)t, \quad y(t) = y_0 + v(x_0, y_0)t, \quad (14)$$

which is called the CV scheme, since the velocity components $[u(x_0, y_0), v(x_0, y_0)]$ are constant during the movement of the Lagrangian drifter inside the ij grid cell.

If the first two terms in the right-hand side of (3) are used, that is,

$$A_x = \left(\frac{\Delta u}{\Delta x}\right)_0, \quad A_y = \left(\frac{\Delta v}{\Delta y}\right)_0, \quad (15)$$

then the two differential equations [(8a) and (8b)] do not depend on (x_1, y_1) and have analytical solutions (Doos 1995; Blanke and Raynaud 1997; Vries and Doos 2001),

$$\begin{aligned} x(t) &= x_0 + \frac{u(x_0, y_0)}{(\Delta u / \Delta x)_0} (e^{A_x t} - 1), \\ y(t) &= y_0 + \frac{v(x_0, y_0)}{(\Delta v / \Delta y)_0} (e^{A_y t} - 1). \end{aligned} \quad (16)$$

It is called the linear uncoupled (LUC) method.

If the first three terms in the right-hand side of (3) are used, that is,

$$\begin{aligned} A_x(x_1, y_1) &= \left(\frac{\Delta u}{\Delta x}\right)_0 + \left(\frac{\Delta u}{\Delta y}\right)_0 \frac{y_1 - y_0}{x_1 - x_0}, \\ A_y(x_1, y_1) &= \left(\frac{\Delta v}{\Delta y}\right)_0 + \left(\frac{\Delta v}{\Delta x}\right)_0 \frac{x_1 - x_0}{y_1 - y_0}, \end{aligned} \quad (17)$$

then the two differential equations [(8a) and (8b)] depend on (x_1, y_1) , which represents the endpoint of the trajectory. It is called the linear coupled (LC) scheme,

since the two velocity components $[u(x_1, y_1), v(x_1, y_1)]$ depend on both x_1 and y_1 linearly. If all the four terms in the right-hand side of (3) are used, that is,

$$A_x(x_1, y_1) = \left(\frac{\Delta u}{\Delta x}\right)_0 + \left(\frac{\Delta u}{\Delta y}\right)_0 \frac{y_1 - y_0}{x_1 - x_0} + \left(\frac{\Delta^2 u}{\Delta x \Delta y}\right)_0 (y_1 - y_0), \quad (18a)$$

$$A_y(x_1, y_1) = \left(\frac{\Delta v}{\Delta y}\right)_0 + \left(\frac{\Delta v}{\Delta x}\right)_0 \frac{x_1 - x_0}{y_1 - y_0} + \left(\frac{\Delta^2 v}{\Delta x \Delta y}\right)_0 (x_1 - x_0), \quad (18b)$$

then the two differential equations [(8a) and (8b)] also depend on (x_1, y_1) . It is called the nonlinear coupled (NLC) scheme, since the two velocity components $[u(x_1, y_1), v(x_1, y_1)]$ depend on both x_1 and y_1 nonlinearly. During the integration of (8a) and (8b), the location (x_1, y_1) is determined from solving the two nonlinear algebraic equations [(12a) and (12b)] using the Newton–Raphson iteration method.

4. Identification of starting grid cell

Let a Lagrangian trajectory start from the initial location (x_{00}, y_{00}) . If

$$x_i < x_{00} < x_{i+1}, \quad (19a)$$

$$y_j < y_{00} < y_{j+1}, \quad (19b)$$

then the point (x_{00}, y_{00}) is located inside the ij grid cell. As the trajectory hits the side or corner of the initial grid cell at the location (x_0, y_0) , it is important to determine which of the next grid cells is for the advance of the trajectory. The location (x_0, y_0) is called the starting point of the next grid cell. The Lagrangian trajectory is always calculated across the grid cell from (x_0, y_0) at the left or right side (Fig. 2), the upper or lower side (Fig. 3), and the grid point (Fig. 4).

Let Fig. 2 be taken as an example for the illustration, since Fig. 3 is similar but in the y direction. For $u_0 \neq 0$ (Fig. 2a), the point (x_0, y_0) is located at the left (right) side and will move to the right (left) grid cell if $u_0 > 0$ ($u_0 < 0$). For $u_0 = 0$ and $v_0 \neq 0$ (Figs. 2b and 2c, respectively), determination of the next grid cell depends on both signs of $[v_0, (\Delta u/\Delta y)_0]$. Solutions (9), (10a), and (10b) require one component of (u_0, v_0) nonzero. For $u_0 = 0, v_0$ must be nonzero. With $v_0 > 0$, the starting point (x_0, y_0) is located in the right cell for $(\Delta u/\Delta y)_0 > 0$ and in the left cell for $(\Delta u/\Delta y)_0 < 0$ (Fig. 2b). With $v_0 < 0$,

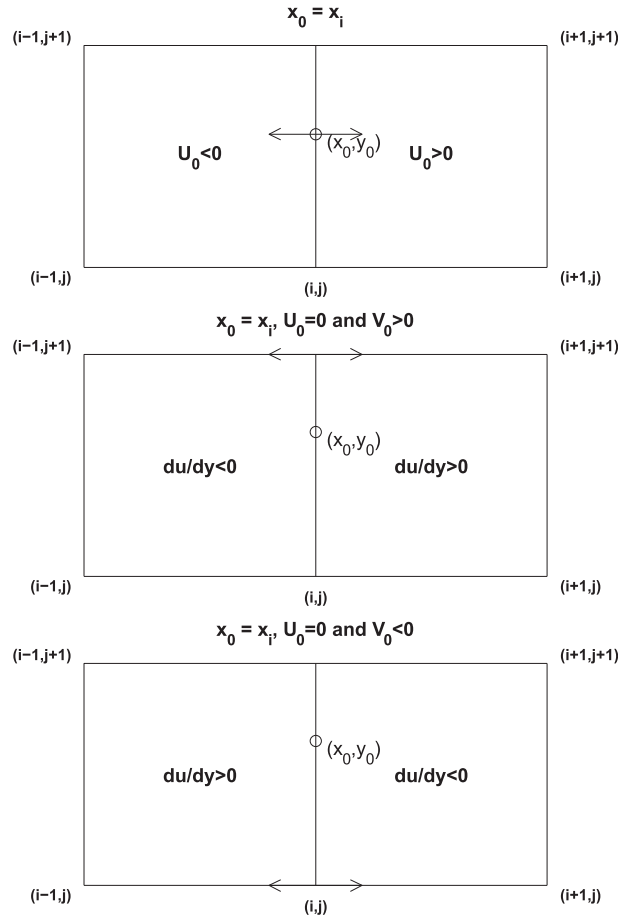


FIG. 2. Determination of the initial grid cell with the initial location of the Lagrangian trajectory (x_0, y_0) located at $x_0 = x_i$ for (a) $u_0 \neq 0$, (b) $u_0 = 0, v_0 > 0$, and (c) $u_0 = 0, v_0 < 0$.

the starting point (x_0, y_0) is located in the right cell for $(\Delta u/\Delta y)_0 < 0$ and in the left cell for $(\Delta u/\Delta y)_0 > 0$ (Fig. 2c). For $u_0 = 0$ and $v_0 = 0$, the trajectory stays at (x_0, y_0) forever.

For (x_0, y_0) located at the corner of the grid cell (i.e., at the grid point such as at $x_0 = x_i, y_0 = y_j$ (Fig. 4), the point (x_0, y_0) will move to the upper-right cell for $(u_0 > 0, v_0 > 0)$, the upper-left cell for $(u_0 < 0, v_0 > 0)$, the lower-left cell for $(u_0 < 0, v_0 < 0)$, and the lower-right cell for $(u_0 > 0, v_0 < 0)$. With $v_0 = 0$, the point (x_0, y_0) will move to the upper-right cell for $[u_0 > 0, (\Delta v/\Delta x)_0 > 0]$, the upper-left cell for $[u_0 < 0, (\Delta v/\Delta x)_0 < 0]$, the lower-left cell for $[u_0 < 0, (\Delta v/\Delta x)_0 > 0]$, and the lower-right cell for $[u_0 > 0, (\Delta v/\Delta x)_0 < 0]$. With $u_0 = 0$, the point (x_0, y_0) will move to the upper-right cell for $[v_0 > 0, (\Delta u/\Delta y)_0 > 0]$, the upper-left cell for $[v_0 > 0, (\Delta u/\Delta y)_0 < 0]$, the lower-left cell for $[v_0 < 0, (\Delta u/\Delta y)_0 > 0]$, and the lower-right cell for $[v_0 < 0, (\Delta u/\Delta y)_0 < 0]$.

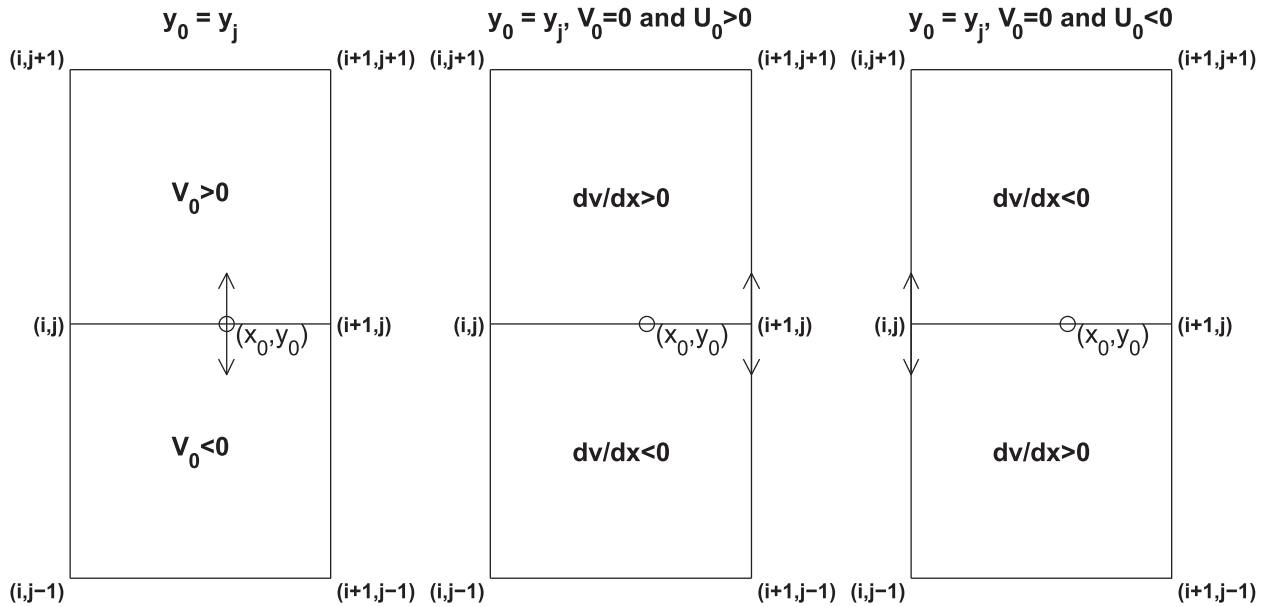


FIG. 3. Determination of the initial grid cell with the initial location of the Lagrangian trajectory (x_0, y_0) located at $y_0 = y_j$ for (a) $v_0 \neq 0$, (b) $v_0 = 0, u_0 > 0$, and (c) $v_0 = 0, u_0 < 0$.

5. Lagrangian trajectory across grid cell

The solutions (9), (10a), and (10b) are valid within a given grid cell. If (x_1, y_1) hits the corner point or side of the grid

cell (x_b, y_b) —that is, $(x_1 = x_b, y_1 = y_b)$ —then this ending point (x_b, y_b) is treated as the starting point for the next grid cell, and is determined by the travel time in the x direction,

$$\tau_x = \begin{cases} \frac{x_b - x_0}{u(x_0, y_0)}, & \text{for } A_x = 0, A_y = 0 \\ \frac{1}{A_x(x_b, y_b)} \ln \left[\frac{(x_b - x_0)A_x(x_b, y_b)}{u(x_0, y_0)} + 1 \right], & \text{for } A_x \neq 0, A_y \neq 0 \end{cases} \quad (20a)$$

and the y direction,

$$\tau_y = \begin{cases} \frac{y_b - y_0}{v(x_0, y_0)}, & \text{for } A_x = 0, A_y = 0 \\ \frac{1}{A_y(x_b, y_b)} \ln \left[\frac{(y_b - y_0)A_y(x_b, y_b)}{v(x_0, y_0)} + 1 \right], & \text{for } A_x \neq 0, A_y \neq 0 \end{cases} \quad (20b)$$

The Lagrangian trajectory hits the corner of the ij grid cell [i.e., one of the four grid points $(x_i, y_j), (x_{i+1}, y_j), (x_{i+1}, y_{j+1})$] if $\tau_x = \tau_y = \tau$. The Lagrangian trajectory hits the side of the cell if $\tau_x \neq \tau_y$. For $\tau_x > \tau_y$, it hits the upper side if $v_0 > 0$ and hits the lower side if $v_0 < 0$. For $\tau_x < \tau_y$, it hits the right side if $u_0 > 0$ and hits the left side if $u_0 < 0$ (Fig. 5).

For the Lagrangian trajectory hitting the cell side, either x_b or y_b takes the gridpoint location (one of $x_i, x_{i+1}, y_j, y_{j+1}$) and the other is obtained from solving an algebraic equation with the constraint of $\tau_x = \tau_y$,

$$v(x_0, y_0)(x_b - x_0) - u(x_0, y_0)(y_b - y_0) = 0, \quad (21a)$$

for the CV scheme,

$$\frac{(x_b - x_0)A_x(x_0, y_0)}{u(x_0, y_0)} - \frac{(y_b - y_0)A_y(x_0, y_0)}{v(x_0, y_0)} = \exp \left[\frac{A_x(x_0, y_0)}{A_y(x_0, y_0)} \right], \quad \text{and} \quad (21b)$$

for the LUC scheme,

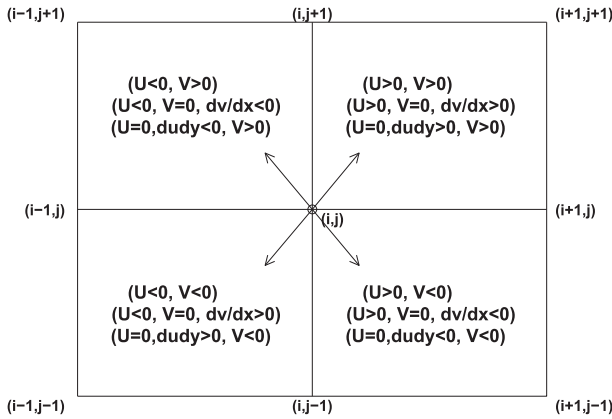


FIG. 4. Determination of the initial grid cell with the initial location of the Lagrangian trajectory (x_0, y_0) located at $x_0 = x_i, y_0 = y_j$.

$$A_y(x_b, y_b) \ln \left[\frac{(x_b - x_0)A_x(x_b, y_b)}{u(x_0, y_0)} + 1 \right] - A_x(x_b, y_b) \ln \left[\frac{(y_b - y_0)A_y(x_b, y_b)}{v(x_0, y_0)} + 1 \right] = 0, \quad (21c)$$

for the LC and NLC schemes. Since one of (x_b, y_b) is given, (21a) and (21b) are linear algebraic equations, which are solved easily and explicitly. However, (21c) is a nonlinear algebraic equation, which is solved using the Newton–Raphson method. After (x_b, y_b) are obtained, the τ is determined, and in turn the Lagrangian trajectory is obtained before hitting the grid cell side (or corner) using (10a) or (10b) for $0 < t < \tau$ (i.e., dashed curve in Fig. 1).

It is also noted that during the integration, the velocity components (u, v) are set to zero under the conditions

$$u = 0 \quad \text{if} \quad \left| \frac{u}{\Delta x} \right| < 10^{-10} \text{ s}^{-1},$$

$$v = 0 \quad \text{if} \quad \left| \frac{v}{\Delta y} \right| < 10^{-10} \text{ s}^{-1}. \quad (22)$$

The relative displacement components $(|x/\Delta x|, |y/\Delta y|)$ are rounded with the accuracy of 10^{-9} .

6. Stommel ocean model on the f plane

Stommel (1948) designed an ocean model to explain the westward intensification of wind-driven ocean currents. Consider a rectangular ocean with the origin of a Cartesian coordinate system at the southwest corner (Fig. 6). The x^* and y^* axes point eastward and northward, respectively. Here, the superscript $*$ denotes dimensional variables. The boundaries of the ocean are at $x^* = 0, \lambda$ and $y^* = 0, b$. The ocean is considered as

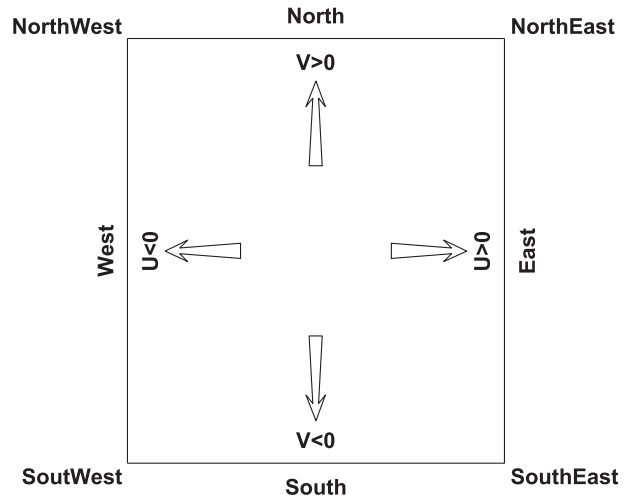


FIG. 5. Determination of the side of the grid cell for the Lagrangian trajectory crossing.

a homogeneous and incompressible layer of constant depth D when at rest. When currents occur as in the real ocean, the depth differs from D everywhere by a small perturbation. Because of the incompressibility, a streamfunction ψ^* is defined by

$$u^* = -\frac{\partial \psi^*}{\partial y^*}, \quad v^* = \frac{\partial \psi^*}{\partial x^*},$$

where u^* and v^* are components of the velocity vector in the x^* and y^* directions. The surface wind stress is taken as $-F \cos(\pi y/b)$. The component frictional forces are taken as $-Ru$ and $-Rv$, where R is the frictional coefficient. The Coriolis parameter f is also introduced. For a constant f , an equation was derived for the streamfunction ψ^* ,

$$\left(\frac{\partial^2}{\partial x^{*2}} + \frac{\partial^2}{\partial y^{*2}} \right) \psi^* = -\gamma \sin \left(\frac{\pi y^*}{b} \right), \quad (23)$$

where $\gamma = F\pi/(Rb)$. The rigid boundary conditions are given by

$$\psi(0, y^*) = \psi(\lambda, y^*) = \psi(x^*, 0) = \psi(x^*, b) = 0. \quad (24)$$

The independent and dependent variables are non-dimensionalized by

$$x = x^*/\lambda - 0.5, \quad y = y^*/b - 0.5, \quad \psi = \psi^* \pi^2 / (\gamma b^2). \quad (25)$$

For simplicity without loss of generality, the dimensional parameters (λ, b) are chosen, such as $\pi\lambda/b = 1$. The analytical solution of (23) in the nondimensional form is given by (Fig. 6b)

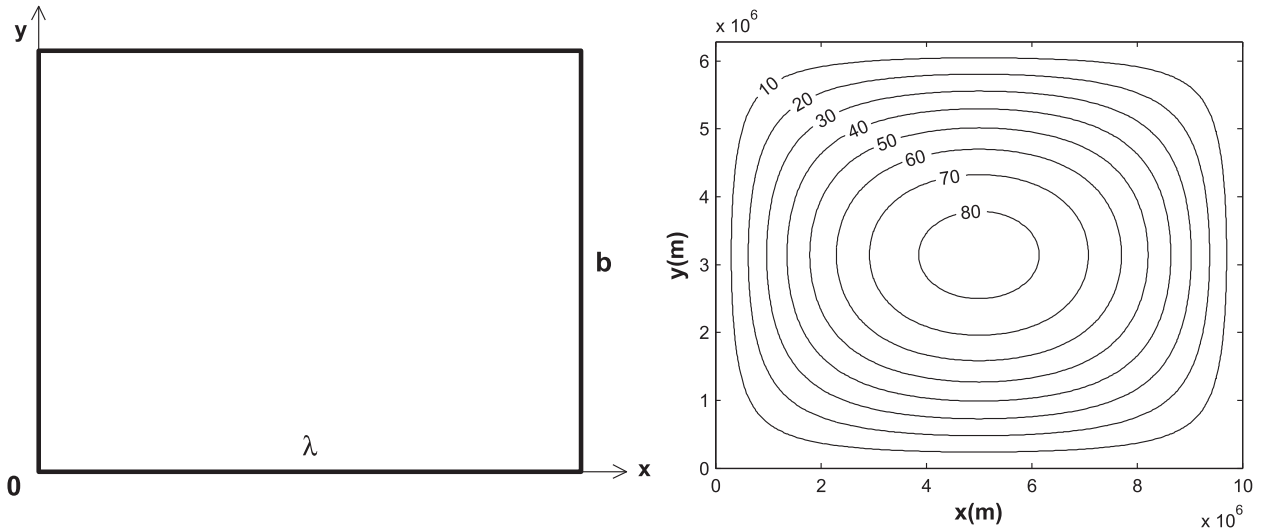


FIG. 6. Stommel ocean model on the f plane: (a) ocean geometry and (b) streamfunction ($\text{m}^2 \text{s}^{-1}$) (after Stommel 1948).

$$\psi(x, y) = \sin(\pi y) \left(1 - \frac{1 - e^{-1}}{e - e^{-1}} e^x - \frac{e - 1}{e - e^{-1}} e^{-x} \right), \quad (26)$$

with $0 \leq x \leq 1$, $0 \leq y \leq 1$ and the maximum value,

$$\psi_{\max} = 1 - 2 \frac{e^{1/2} - e^{-1/2}}{e - e^{-1}}. \quad (27)$$

The nondimensional velocity components of the Stommel model (u_s, v_s) are given by

$$\begin{aligned} u_s(x, y) &= -\frac{\partial \psi}{\partial y} \\ &= -\pi \cos(\pi y) \left(1 - \frac{1 - e^{-1}}{e - e^{-1}} e^x - \frac{e - 1}{e - e^{-1}} e^{-x} \right), \\ v_s(x, y) &= \frac{\partial \psi}{\partial x} = -\sin(\pi y) \left(\frac{1 - e^{-1}}{e - e^{-1}} e^x - \frac{e - 1}{e - e^{-1}} e^{-x} \right). \end{aligned} \quad (28)$$

7. Accuracy progressive among the four schemes

The nondimensional ocean basin is discretized by $\Delta x = \Delta y = 0.02$. The velocity components are calculated at the grid points $(u_{i,j}, v_{i,j})$ ($i = 1, 2, \dots, 51; j = 1, 2, \dots, 51$) using (28). With the gridded Eulerian velocity fields $(u_{i,j}, v_{i,j})$, the continuous velocity fields $[u(x, y), v(x, y)]$ are obtained using (6) with four different methods (CV, LUC, LC, and NLC). Since the Stommel model on the f plane is symmetric (Fig. 6), the initial location is selected by

$$x_{00} = 0.14, \quad y_{00} = 0.0, \quad (29)$$

which is 2.5 times away from the boundary than from the center of the circulation. Equation (26) shows that the streamfunction at (x_0, y_0) is given by

$$\psi_0 = \psi(0.14, 0.0) = 0.1045. \quad (30)$$

Since the Stommel ocean model has the steady-state analytical solution, the Lagrangian drifter is supposed to move along any closed streamline (Fig. 7a), which means that the Lagrangian trajectory coincides with the streamline and should be closed. The two differential equations [(8a) and (8b)] are integrated using the four schemes (CV, LUC, LC, NLC) for computing $A_x(x, y)$ and $A_y(x, y)$ with the Lagrangian trajectory moving around the ocean basin up to 100 circles.

First, the analytical streamline (Fig. 7a) is used to evaluate the accuracies of the CV, LUC, LC, and NLC schemes (Figs. 7b–e). The Lagrangian trajectory is not a closed circle using the CV, LUC, and LC schemes: using the CV scheme, it hits the ocean boundary after 8.375 circles (Fig. 7b); using the LUC scheme, it hits the ocean boundary after 26 circles (Fig. 7c); using the LC scheme, it does not hit the ocean boundary after 100 circles (but not a closed streamline with the ψ value changing to 0.032 after 100 circles) (Fig. 7d). However, using the NLC scheme, it is exactly the same as the analytical streamline after 100 circles (ψ value kept as 0.1045) (Fig. 7e). Since $\psi = 0$ at the lateral boundary, the following criterion

$$|\psi| \leq 10^{-6} \quad (31)$$

is used to identify the Lagrangian trajectory hitting the lateral boundary.

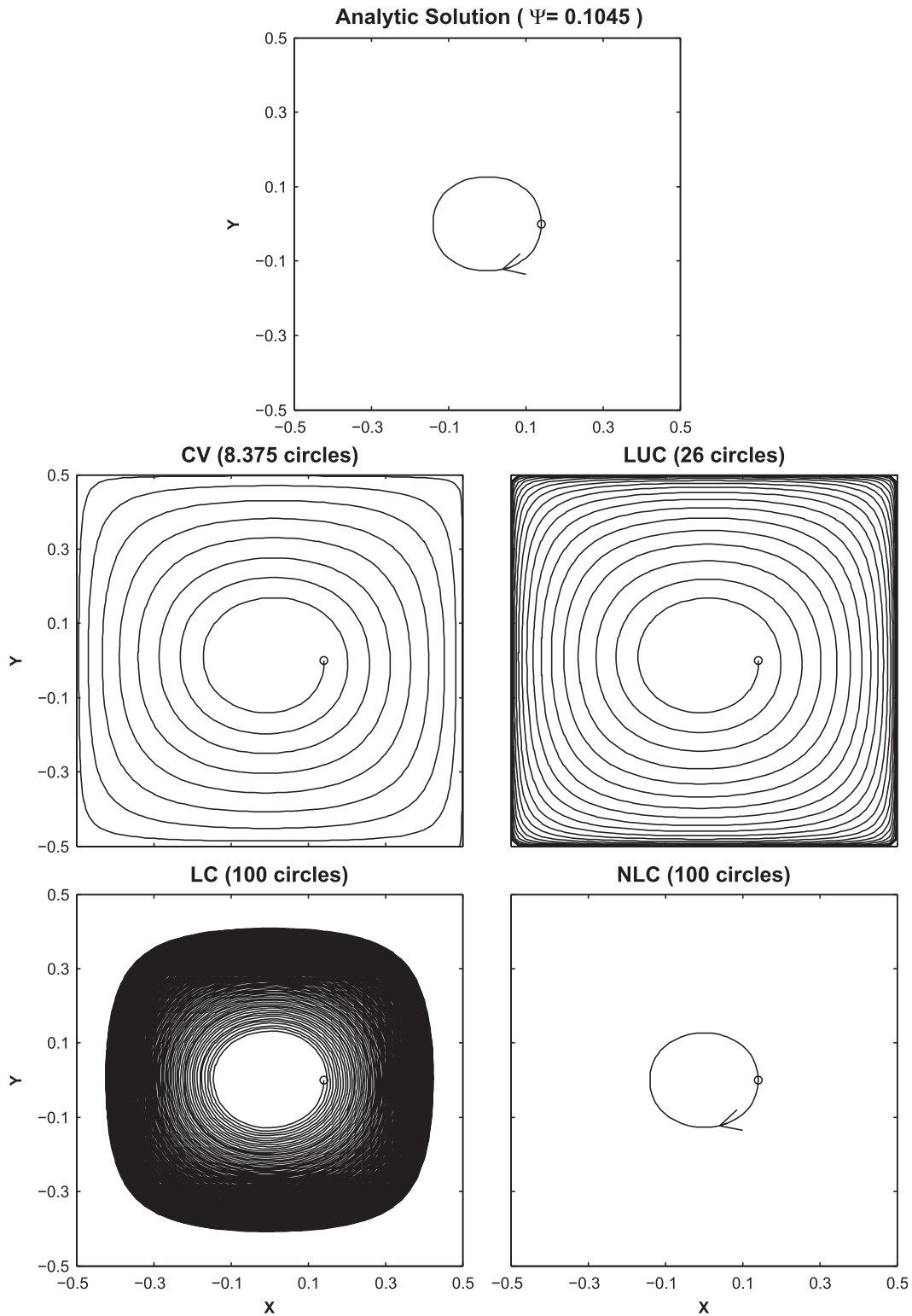


FIG. 7. Calculated Lagrangian trajectories with the initial location (0.14, 0.00) and $\psi_0 = 0.1045$ using (a) analytical solution, (b) CV scheme, (c) LUC scheme, (d) LC scheme, and (e) NLC scheme.

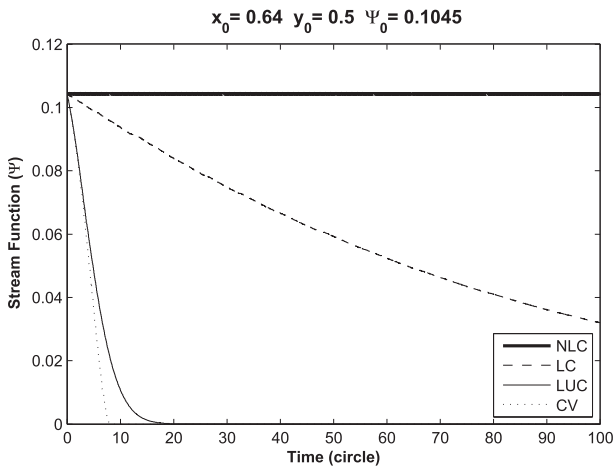


FIG. 8. Temporal evolution of ψ values of the Lagrangian trajectory calculated with the four schemes. Noted that the time is represented by the number of circles around the ocean basin.

Second, the initial streamfunction ψ_0 is used to evaluate the four methods. The smaller the difference of the numerical ψ value against ψ_0 , the more accurate the scheme would be. Figure 8 shows the dependence of the ψ value versus the circle of the Lagrangian trajectory around the ocean basin. The zero value of the streamfunction indicates the ocean boundary. The ψ value reduces from 0.1045 to 0 at the 8.375th (26th) circle using the CV (LUC) method, and to 0.032 at the 100th circle using the LC method. The ψ value stays at 0.1045 after 100th circle using the NLC method.

Third, the relative root-mean-square error (RRMSE) of the streamfunction is used to evaluate the accuracy,

$$RRMSE = \frac{|\psi - \psi_a|}{\psi_a}, \quad (32)$$

where ψ_a is the analytical streamfunction. The comparison is conducted with three different initial locations (Table 1) with associated ψ_a values (0.1045, 0.087 52, 0.061 43) (Fig. 9). For the same initial location (x_{00}, y_{00}) , RRMSE increases from 0 to 1.0 in 5–8 circles using the CV method, it is in 17 circles using the LUC method, and it increases from 0 to around 0.7 in 100 circles using the LC method. RRMSE keeps near 0 in 100 circles using the NLC scheme (Fig. 10a). For the same method, RRMSE increases as the initial location changes toward the boundary (from case 1 to case 3 in Table 1). To further investigate the performance of the NLC method, RRMSE (in 10^{-3}) is plotted in one circle for the three initial locations (Fig. 10b). The oscillation of RRMSE is noted with the largest (smallest) amplitude for case 3 (case 1). The minimum RRMSE values occur when the trajectory passing four points $(0, y_{\pm})$,

TABLE 1. Three initial locations and associated analytical ψ_a values.

Case	x_0	y_0	ψ_a value
1	0.14	0.0	0.1045
2	0.24	0.0	0.087 52
3	0.34	0.0	0.061 43

$(x_-, 0)$, $(0, y_+)$, $(x_+, 0)$ with either $u = 0$ or $v = 0$. The 2D calculation becomes a 1D calculation and greatly decreases the RRMSE.

The CPU time comparison is based either on the first 5 circles (Table 2) or the first 100 circles (or hitting the boundary) (Table 3) of the Lagrangian drifter around the streamline of the Stommel model. Since the Stommel model is steady state, the Lagrangian trajectory coincides with the Eulerian streamline. The calculated Lagrangian trajectory has less (more) deviation to the streamline using a more (less) accurate scheme with accuracy decreasing from the NLC, LC, and LUC scheme to the CV scheme (see Fig. 7). Thus, the Lagrangian drifter moves the shortest distance per circle using the NLC scheme and the longest distance using the CV method. Except for the CV scheme (consuming the least amount of CPU time—0.0031 s per circle), for the first 5 circles the NLC scheme consumes less CPU time per circle (0.034 32 s) than the LUC scheme (0.065 52 s) and the LC scheme (0.037 44 s) (Table 2), and up to 100 circles (or hitting the boundary); the NLC scheme consumes a comparable CPU time

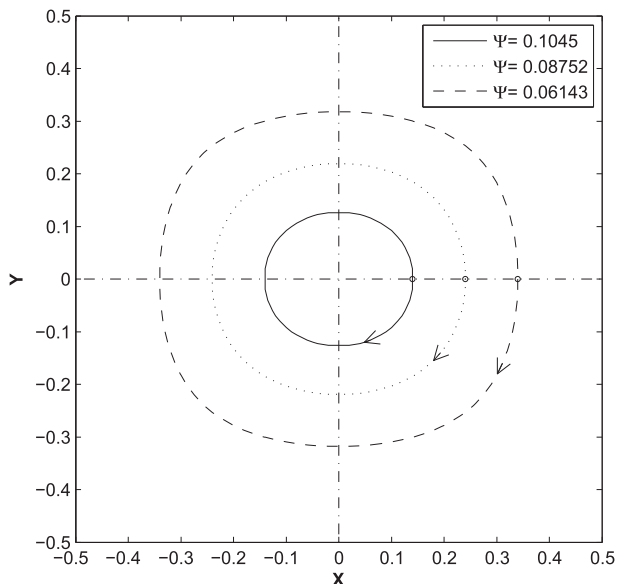


FIG. 9. Streamlines with three different initial locations: (0.14, 0.00) (solid curve, $\psi_0 = 0.1045$), (0.24, 0.00) (dotted curve, $\psi_0 = 0.08752$), and (0.34, 0.00) (dashed curve, $\psi_0 = 0.06143$).

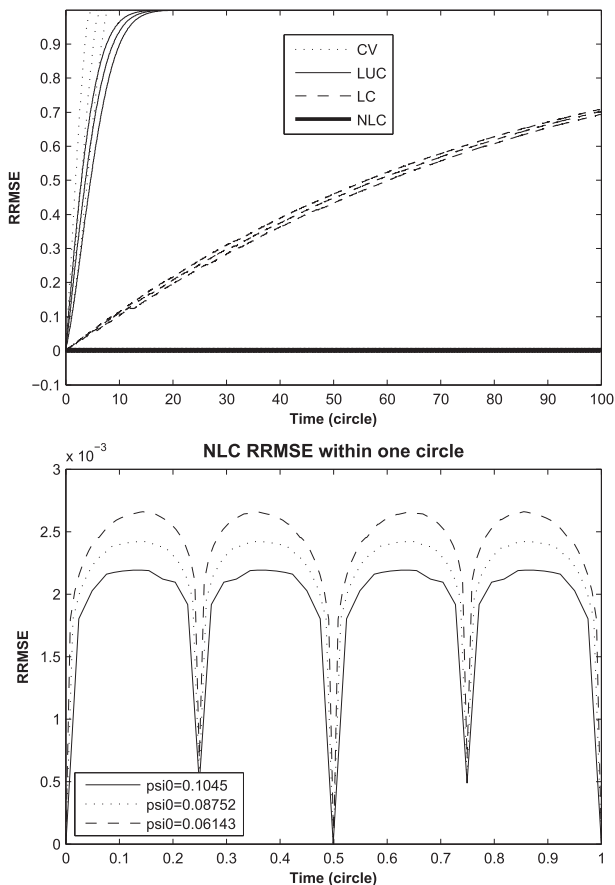


FIG. 10. (a) Temporal evolution of RRMSE of the streamfunction of the Lagrangian trajectory calculated with the four schemes using the four schemes with three different initial locations. (b) Zoom-in temporal evolution of RRMSE of the streamfunction of the Lagrangian trajectory calculated with the NLC scheme (vertical scale is nearly three orders of magnitude smaller). It is noted that the time is represented by the number of circles around the ocean basin.

per step (0.000 660 s) as the LUC scheme (0.000 636 s) and the LC scheme (0.000 064 6 s). The lowest CPU time per circle and per step using the CV scheme is caused by the simplest calculation of the Lagrangian trajectory [i.e., Eq. (9)].

TABLE 2. Comparison of CPU (s) for the first five circles among the four methods.

	CV	LUC	LC	NLC
CPU for five circles	0.0156	0.3276	0.1872	0.1716
CPU per circle	0.0031	0.065 52	0.037 44	0.034 32

8. Conclusions

- Two sources of uncertainty in determining the Lagrangian trajectories from the Eulerian velocity are identified: (i) the knowledge of the smoothness and (ii) the error in the integration of the ordinary differential equations. This study especially shows the process of establishing a series of accuracy progress schemes (CV, LUC, LC, NLC) with different knowledge of smoothness for calculating Lagrangian trajectory using the gridded velocity field through different truncations of a two-dimensional interpolation. All four schemes are within the same analytical framework using two coefficients (A_x, A_y) with the time dependence of the Lagrangian trajectory analytical: linear for the CV scheme, and exponential for the remaining schemes (LUC, LC, NLC).
- Accuracy increases with the change of the two coefficients (A_x, A_y). When $A_x = A_y = 0$, the Lagrangian velocity components use the starting velocity (u_0, v_0) (the CV scheme), and the accuracy is the lowest. When (A_x, A_y) are truncated at the first term of the right-hand side in (7), the Lagrangian velocity component u depends on x , and v depends on y only (the LUC scheme), and the accuracy is the lower. When (A_x, A_y) are truncated at the first two terms of the right-hand side in (7), the Lagrangian velocity components (u, v) depend on (x, y) linearly (the LC scheme), and the accuracy is higher. When (A_x, A_y) keep all three terms of the right-hand side in (7), the Lagrangian velocity components (u, v) depend on (x, y) nonlinearly (the NLC scheme), and the accuracy is at its highest. The Lagrangian trajectory is obtained explicitly using the CV and LUC schemes, and implicitly using the LC and NLC schemes with the Newton–Raphson iteration method.

TABLE 3. Comparison of CPU (s) for the Lagrangian trajectories either hitting the boundary or up to 100 circles among the four methods.

	CV	LUC	LC	NLC
Circles either hitting the boundary or 100 circles	8.375	26	100	100
Total CPU	0.0312	2.8704	8.2057	3.6036
CPU per circle	0.0037	0.1104	0.0821	0.0360
Total steps	1176	4517	12 696	5200
CPU per step	0.000 026 5	0.000 636	0.000 646	0.000 660

- 3) The nondimensional (length of 1.0 in both x and y directions) Stommel ocean model (steady state with analytical solution) on the f plane is used for the evaluation. The Lagrangian trajectory is calculated from the initial location at the distance of 0.14 to the center of the ocean basin using the four schemes (CV, LUC, LC, and NLC) from the gridded velocity data obtained from the analytical Stommel ocean model. The Lagrangian trajectory is accurately determined with no deviation from the streamline even after the Lagrangian drifter is moving around the ocean basin after 100 circles using the NLC scheme; less accurately determined with deviation from the streamline using the LC scheme; inaccurately determined with evident deviation from the streamline (hitting the ocean boundary after 26 circles) using the LUC scheme; and very inaccurately determined with a large deviation from the streamline (hitting the ocean boundary after 8.375 circles) using the CV scheme. The CV scheme consumes the least amount of CPU time. The NLC scheme consumes a comparable amount of CPU time as do the LUC and LC schemes.
- 4) High accuracy with no evident increase in the amount of CPU time makes the NLC scheme a promising scheme for calculating Lagrangian trajectory from gridded velocity data, especially with strongly curved streamlines.
- 5) Calculation of Lagrangian trajectories from the 2D gridded velocity field described here is easy to extend to the 3D gridded velocity field by changing the 2D grid cell into the 3D grid volume. For the procedure identified in section 4, the trajectory starts from a surface (or grid point) of the grid volume (x_0, y_0, z_0) rather than a side (or grid point) of the grid cell (x_0, y_0), and ends at a surface (or grid point) (x_b, y_b, z_b) rather than a side (or grid point) of the grid cell (x_b, y_b). The starting point for the next grid volume is determined by equalizing the three travel times (τ_x, τ_y, τ_z) [similar to (20a), and (20b)], $\tau_x = \tau_y = \tau_z$, which provides two algebraic equations of (y_b, z_b) for the CV scheme [similar to (21a)], the LUC scheme [similar to (21b)], and the LC and NLC schemes [similar to (21c)]. The two algebraic equations are solved by the 2D Newton-Raphson method.
- 6) The semi-Lagrangian method combines both the Eulerian and Lagrangian points of view. The fluid variable is discretized on an Eulerian grid but is advanced in time using the equation similar to (2a). The algorithms in the context of calculations of drifter trajectories (e.g., the CV, LUC, LC, NLC schemes) can be applied to the semi-Lagrangian methods in ocean modeling.
- 7) The limitation of this study is that only an analytical steady ocean model—that is, the Stommel model—is used for evaluating the four schemes. In the context of practical application to the trajectories of drifters driven by oceanographic fields, it will be useful to examine the properties of these algorithms in the near future under somewhat more realistic conditions—for instance, output from an eddy-resolving ocean model (i.e., an unsteady Eulerian gridded flow field).

Acknowledgments. This research was supported by the Office of Naval Research (Grant N0001413AF00002) and the Naval Oceanographic Office (Grant N6230612PO00123).

REFERENCES

- Blanke, B., and S. Raynaud, 1997: Kinematics of the Pacific Equatorial Undercurrent: An Eulerian and Lagrangian approach from GCM results. *J. Phys. Oceanogr.*, **27**, 1038–1053, doi:10.1175/1520-0485(1997)027<1038:KOTPEU>2.0.CO;2.
- Chu, P. C., and C. W. Fan, 2010: Space-time transformation in flux-form semi-Lagrangian schemes. *Terr. Atmos. Oceanic Sci.*, **21**, 17–26, doi:10.3319/TAO.2009.05.25.01(IWNOP).
- , S. H. Lu, and Y. C. Chen, 2001: Evaluation of the Princeton Ocean Model using the South China Sea Monsoon Experiment (SCSMEX) data. *J. Atmos. Oceanic Technol.*, **18**, 1521–1539, doi:10.1175/1520-0426(2001)018<1521:EOTPOM>2.0.CO;2.
- , L. M. Ivanov, T. P. Korzhova, T. M. Margolina, and O. V. Melnichenko, 2003a: Analysis of sparse and noisy ocean current data using flow decomposition. Part I: Theory. *J. Atmos. Oceanic Technol.*, **20**, 478–491, doi:10.1175/1520-0426(2003)20<478:AOSANO>2.0.CO;2.
- , —, —, —, and —, 2003b: Analysis of sparse and noisy ocean current data using flow decomposition. Part II: Application to Eulerian and Lagrangian data. *J. Atmos. Oceanic Technol.*, **20**, 492–512, doi:10.1175/1520-0426(2003)20<492:AOSANO>2.0.CO;2.
- , G. H. Wang, and C. W. Fan, 2004: Evaluation of the U.S. Navy's Modular Ocean Data Assimilation System (MODAS) using the South China Sea Monsoon Experiment (SCSMEX) data. *J. Oceanogr.*, **60**, 1007–1021, doi:10.1007/s10872-005-0009-3.
- , L. M. Ivanov, and O. V. Melnichenko, 2005: Fall–winter current reversals on the Texas–Louisiana continental shelf. *J. Phys. Oceanogr.*, **35**, 902–910, doi:10.1175/JPO2703.1.
- , —, —, and N. C. Wells, 2007: On long baroclinic Rossby waves in the tropical North Atlantic observed from profiling floats. *J. Geophys. Res.*, **112**, C05032, doi:10.1029/2006JC003698.
- Doos, K., 1995: Inter-ocean exchange of water masses. *J. Geophys. Res.*, **100**, 13 499–13 514, doi:10.1029/95JC00337.
- Galanis, G., P. Louka, P. Katsafados, I. Pytharoulis, and G. Kallos, 2006: Applications of Kalman filters based on non-linear functions to numerical weather predictions. *Ann. Geophys.*, **24**, 2451–2460, doi:10.5194/angeo-24-2451-2006.
- Gandin, L. S., 1965: *Objective Analysis of Meteorological Fields*. Israel Program for Scientific Translation, 242 pp.
- Lozano, C. J., A. R. Robinson, H. G. Arango, A. Gangopadhyay, Q. Sloan, P. J. Haley, L. Anderson, and W. Leslie, 1996: An

- interdisciplinary ocean prediction system: Assimilation strategies and structured data models. *Modern Approaches to Data Assimilation in Ocean Modeling*, P. Malanotte-Rizzoli, Ed., Elsevier Oceanography Series, Vol. 61, 413–452, doi:[10.1016/S0422-9894\(96\)80018-3](https://doi.org/10.1016/S0422-9894(96)80018-3).
- Song, Y. T., and F. Colberg, 2011: Deep ocean warming assessed from altimeters, Gravity Recovery and Climate Experiment, in situ measurements, and a non-Boussinesq ocean general circulation model. *J. Geophys. Res.*, **116**, C02020, doi:[10.1029/2010JC006601](https://doi.org/10.1029/2010JC006601).
- Stommel, H. M., 1948: The westward intensification of wind-driven ocean currents. *Trans. Amer. Geophys. Union*, **29**, 202–206, doi:[10.1029/TR029i002p00202](https://doi.org/10.1029/TR029i002p00202).
- Sun, L. C., 1999: Data inter-operability driven by oceanic data assimilation needs. *Mar. Technol. Soc. J.*, **33**, 55–66, doi:[10.4031/MTSJ.33.3.7](https://doi.org/10.4031/MTSJ.33.3.7).
- Vries, P. D., and K. Doos, 2001: Calculating Lagrangian trajectories using time-dependent velocity fields. *J. Atmos. Oceanic Technol.*, **18**, 1092–1101, doi:[10.1175/1520-0426\(2001\)018<1092:CLTUTD>2.0.CO;2](https://doi.org/10.1175/1520-0426(2001)018<1092:CLTUTD>2.0.CO;2).